RSC Advances

ROYAL SOCIETY OF CHEMISTRY

www.rsc.org/advances

Journal Name

ARTICLE

In Situ Transmission Electron Microscopy of Ag-Incorporated Carbon Nanofibers: Study on Ag Nanoparticles Size behavior to the Graphene Formation.

Yazid Yaakob[a,b], Mohd Zamri Mohd Yusop[a,c], Chisato Takahashi[d], Mohamad Saufi Rosmi[a,e], Golap Kalita[a], and Masaki Tanemura[a,]*

We have studied the graphene formation from a single Ag-incorporated carbon nanofiber (CNF) during electrons emission process by in situ transmission electron microscopy (TEM) facilities. Graphene formation from the Ag-incorporated CNF structure was observed under high current flow between 900 nA to 2.03 µA during the field and thermal electrons emission. The Joule heating generated the risen temperature which estimated approximately 440 to 1030 K, leads the amorphous carbon that surrounding Ag particles transformed significantly to graphene structure, and the evaporation of Ag particles occurred almost simultaneously. The evaporation of Ag particles interrupt the thermal electron emission process thus decreasing the emission current to ~300 nA. The graphene formation also suspended after Ag particles evaporation occurred. In this paper we will discuss the Ag particles size effect as the catalyst for high quality graphene fabrication.

Introduction

Graphene, a two-dimensional monolayer sheet of carbon with honeycomb lattice structure, has attracted great interest due to its magnificent mechanical, electrical and chemical properties.[1-5] These unique properties make them promising candidates to replace current materials in various applications.[6-8] In order to explore its practical applications, numerous approaches have been developed to synthesis graphene in large scale with controllable integration of its layer. One of the popular methods for the graphene growth is chemical vapor deposition (CVD). In CVD, high quality graphene can be grown on a variety of metal substrates which will act as catalysts, especially on nickel (Ni), cobalt (Co), and copper (Cu).[9-13] Recently, there were also reports of graphene growth on a bulk surface of noble metals such as gold (Au) and silver (Ag), which were assumed to be the metals with poor catalytic activity in CVD.[14,15] This indicates the possibilities and potential to growth and combine graphene with various kind of metals.

In our previous reports, we have demonstrated that carbon nanofibers (CNFs) grow simply by Ar^{+} ion irradiation onto the carbon surface even at room temperature and that any metal can be readily incorporated into the ion-induced CNFs by a simultaneous metal supply during CNF growth.[16-19] In situ transmission electron microscopy (TEM) studies revealed that the structure transformation of the metal incorporated CNF was induced by high electron current flow along the CNF during the field emission (FE) process. In iron (Fe) and gold (Au) incorporated CNFs case, for instance, structural changes from amorphous CNF to bamboo-like CNT and hollow graphitic structure were observed, respectively.[20,21] In contrast, pristine CNFs without any metal incorporation showed totally different structural behavior, where the amorphous CNF was transformed to unorganized ring-like stack of graphitic structure.[22] They are examples of the in situ observation of the crystalized nanocarbon formation by the solid phase reaction. Thus, in situ TEM will possess a great potential to reveal the growth mechanism of graphene formation in nanoscale.

Ag possesses excellent electrical, thermal and optical properties, making them indispensable in various kinds of fields. It has been also demonstrated that the combination of Ag nanoparticles with nanocarbon materials like CNFs and graphene can enhance their field electron emission, electrical, and photoresponce properties.[19,23,24] Based on these background, in what follows, we will challenge to investigate the graphene growth directly from Ag-incorporated CNF induced by electron emission current by using in situ TEM.

Experimental Methods

Figure 1(a) shows a schematic images of sample setup for the Ag-incorporated CNFs. Samples were prepared on commercially available graphite foils (5 mm × 10 mm × 100 μm in thickness) by ion irradiation method, using Kaufmann-type ion gun (Iontech. Inc. Ltd., model 3-1500-100FC). In this process, Ag plate was placed perpendicularly to the graphite foil as Ag source. Both the carbon foil and the Ag plate were co-sputtered with Ar^+ at ion incidence angle of 45° from normal to the carbon and Ag surfaces. The sample fabrications were carried out for 60 min at room temperature. The ion beam employed was 6 cm in diameter, with energy and current density of 600 eV and 6.0 mA/cm^2, respectively. The basal and working pressure were 1.5×10^{-5} and 2.0×10^{-2} Pa, respectively. Surface morphology of the sample was observed carefully by scanning electron microscope (SEM, JEOL JEM-5600). Figure 1(b) disclosed that the Ag-incorporated CNFs grew on the tips of conical protrusions. It should be noted that only one CNF grown on every respective conical protrusion. Then, the sample was cut into 2 mm width and directly mounted of the TEM holder for the in-situ TEM observation (JEOL JEM-2010HR). The sample was mounted as a cathode on a stationary stage while a platinum-iridium (Pt-Ir) nanoprobe as an anode on a piezo-driven stage of TEM specimen holder (JEOL; EM-Z02154T), as illustrated in Figs 1(c). Electrons emission measurements of the single Ag-incorporated CNFs were carried out in working pressure of 1×10^{-5} Pa. The microscope was operated at an acceleration voltage of 200 kV. TEM images were continuously recorded using a CCD camera and an image recording application. While observing the sample structural behavior, the electrons emission current were measured and controlled by changing the bias voltage.
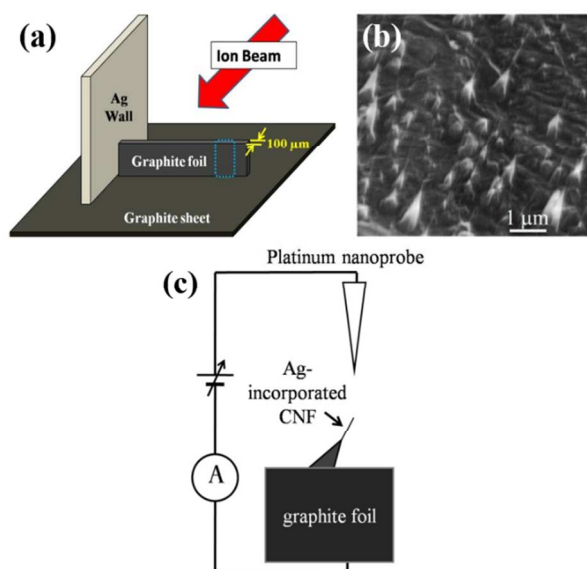

Fig 1 (a) Schematic diagram of the experimental setup for Ag-incorporated CNFs fabrication. Inset circle area were the sample employed for in situ TEM experiment. (b) SEM image of Ag-incorporated CNFs at graphite edge. (c) Schematic diagram of the in situ FE measurement experimental setup.

Results and Discussion.

Figures 2(a)-(c) show the high resolution TEM images of single Ag-incorporated CNF. In figure 2(a), the fiber was observed to be approximately 960 nm in length and 10 nm in diameter. Figures 2(b)-(c) show high-magnification image of cone (base) and middle area of the Ag-CNF, respectively. The image reveals that fine Ag crystallites with 5 – 15 nm in diameter were well dispersed in the amorphous carbon CNF matrix. The selected area electron diffraction (SAED) pattern and energy-dispersive X-ray spectrometry (EDS) of the CNF at the A area are shown in Fig. 3(a) and (b), respectively. The diffraction shows polycrystalline ring pattern of Ag, which indicates that the Ag incorporated CNF contain a mixture of amorphous carbon and randomly oriented Ag crystallites, that was confirmed with the EDS results.
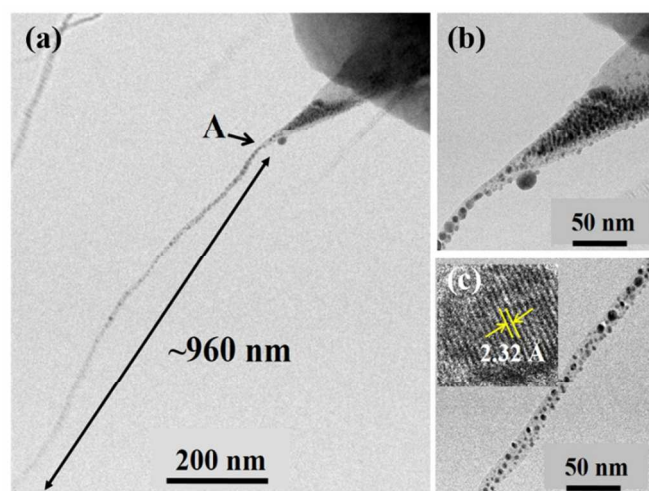

Fig 2 (a) TEM image of the initial Ag-incorporated CNF used for FE measurement. High-magnification images of the fiber as pointed by the arrow : (b) base area and (c) middle area. The inset shows high magnification of Ag particle
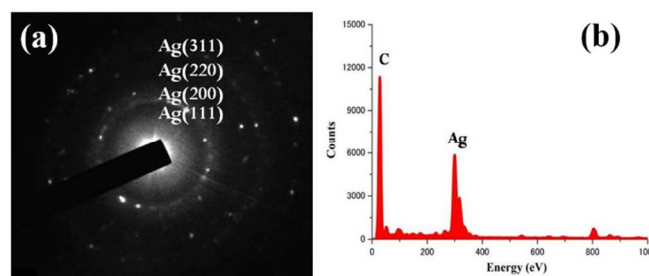

Fig. 3 (a) SAED pattern and (b) EDS spectra of the Ag-incorporated CNF taken for A area.

The influence of the electron emission process on the structure of Ag-incorporated CNF was investigated in situ by FE measurement in a TEM. The distance gap between the Ag-incorporated CNF

(cathode) and platinum nanoprobe (anode) was set to be 1.5 μm. Bias voltage was applied to 150 V with incremental steps of 10 V while observing the fiber at × 150k magnification. Figure 4 shows the FE properties (current-voltage) curves of a single Ag-incorporated CNF. The highest emission current value obtained was 2.03 μA at 100 V/μm. From the current-voltage graph curves, FE characteristics were analyzed using a Fowler-Nordheim (F-N) plot, which can be calculated from F-N equation (1),

$$I = \frac{k_1 A F^2}{\varphi} exp\left(-k_2 \frac{\varphi^{3/2}}{F}\right) \qquad (1)$$

where k_1= 1.54 ×10^{-6}A eV V^{-2}, k_2= 6.83 ×10^9eV$^{-3/2}$ Vm^{-1}, I is the emission current, A is the emission area, and φ is the work function. The local electrical field F is usually proportional to voltage V as equation (2) [25],

$$F = \frac{\beta V}{d} \qquad (2)$$

where β is the field enhancement factor. Here, β can be estimated from the slope of the F-N plot. The β value was calculated to be 31, assuming a work function of 4.6 eV for graphite. This β value was smaller than the value reported from single Fe-incorporated CNF and CNT,[20,26] due to the anode-cathode distance,d was smaller in this case.

Figures 5(a) ~ (c) show the TEM images of the Ag-incorporated CNF after electrons emission measurement. Figure 5(a) reveal that the apex of the fiber moved toward anode direction owing to charge effect during electron emission process. Moreover, a significant structural transformation of the fiber part was observed compared to Fig. 2. As shown in Figs. 5(a) ~ (c), Ag particles that incorporated along the fiber disappeared, leaving hole in the fiber after electron emission process. The SAED analysis at the A area in Fig. 5(a) after electron emission process show ring pattern (inset), indicating that the structures was in very fine polycrystalline nature. However, only diffraction ring pattern of carbon length were obtained while Ag diffraction length were unspotted. This SAED results clarify the absence of Ag particles in CNF and the graphitization of amorphous carbon, at the respective area. To confirm this, higher magnification TEM observation has been performed. Figures 6(a) and 6(b) show comparison of higher magnification TEM images which taken from A area of the fiber before and after the electron emission process. The comparison reveal that the Ag particles in the fiber were evaporated leaving holes with the similar shape of the Ag particles. Furthermore, amorphous carbon around the silver particles were transformed to graphene-like structure owing to Joule heating induced by emission current flow during electron emission process.[27] The high magnification TEM shows that the lattice spacing between layers was around 3.47Å, consistent with that of graphite. The elevated temperature of one dimensional (1-D) object like CNF can be estimated by using a resistive heating model.[28] The temperature distribution equation(3) is,
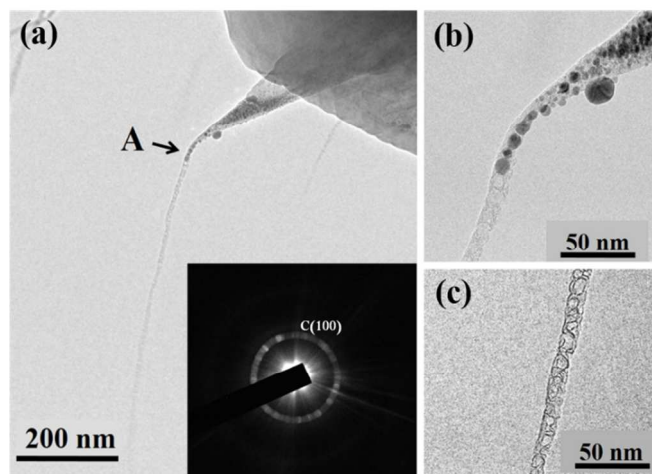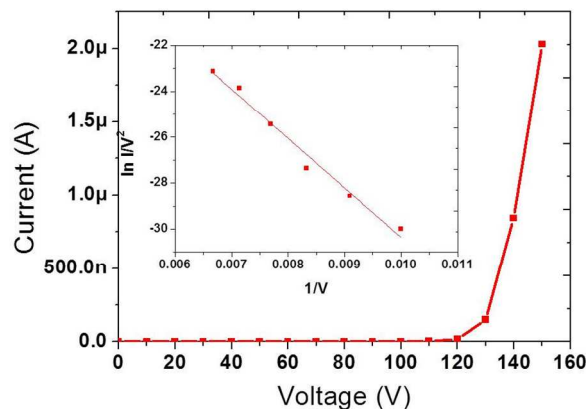
Fig. 4.   Field emission I-V curves and F-N plot (inset) of the Ag-incorporated CNF.

$$T(L) - T_0 = \Delta T_A = \frac{RLI^2}{2\kappa A} \qquad (3)$$

Fig. 5.   (a) TEM image of Ag-incorporated CNF after FE measurement. High-magnification images of the fiber as pointed by the arrow: (b) base area and (c) middle area. The inset shows the SAED pattern of the fiber.
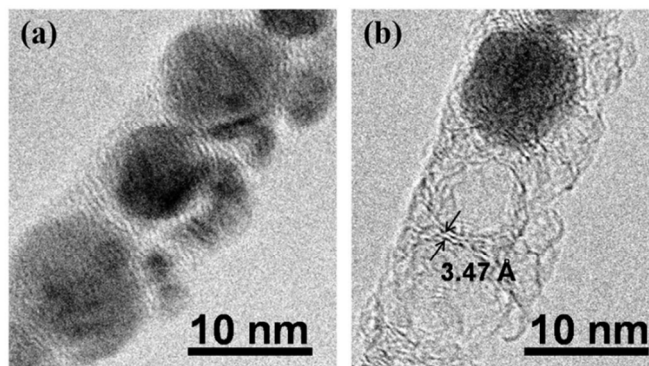

Fig. 6.   High magnification images taken from A area (a) before and (b) after the FE process. The arrow indicate the graphitization of the carbon around silver particle.

where κ is the thermal conductivity (100 W/mK), A is the cross section of the fiber, R is the resistivity of CNT/CNF (2.0×10^6 Ω·m), L is the length of the fiber, and I is the emission current. Here, we considering the emitter length, L to be the total distance from the fiber apex to the cone base, L was measured to be 1.4 µm. As shown in Fig. 4, the maximum emission current, I soared to 2.03 µA. At this point, the temperature of the fiber was estimated to reach 1030 K, which will enhance the graphitization through carbon diffusion around the Ag particles. This explanation were further supported by SAED results in Fig. 5(a) inset which shows polycrystalline ring pattern that representing the graphitic structure.[29] The evaporation of bulk Ag under high vacuum pressure at 1×10^{-5} Pa already started at 850 K, which have been reported by Jones *et al.*[30,31] Thus, we believed that the Ag particles which disappeared were evaporated due to the escalated temperature, as Ag evaporation could occur in TEM working pressure at temperature below 1000 K. One more factor that can be consider were the size effect on the melting temperature of Ag in nano size particles compared to the bulk size, where Ag nanoparticles melting point should be lower compare to usual bulk Ag.[32,33] Hence, the Ag nanoparticles in our case also believed to be evaporated at temperature below 1000 K. The graphitization was occurred due to surface adsorption of carbon atoms on Ag particles.[34] Since the Ag particles evaporation and the graphitization process occurred almost simultaneously by Joule heating, it leave an imperfect graphitic structure on the surface while maintaining the hole similar to the Ag particles shape.

The TEM images of the fiber structural behavior at A area are shown in Figure 7. The images of Figs. 7(a)-(f) were the images series of a motion of the nanofiber structural change during emitting electrons at high current. The applied voltage was increased gradually from 130 V to 150 V. At 130 V bias voltage the emission current ~150 nA was obtained. During this period, there were no significant changes of the fiber structure can be observed. Then, the applied voltage increased to 140 V, the current drastically increased to ~800 nA. At this emission current, significant changes in the structure of the Ag incorporated CNF was observed as shown in Figs. 7(a)-(e). As pointed by the arrow, it can be seen that the Ag particles were evaporated gradually starting from apex to base of the CNF. The focused electrons emitting through the apex triggered the Joule heating which later the risen temperature channeled to the base of the CNF. This can be understand as the sharp apex area has larger electric field compared to the base of the CNF. When the applied voltage increased to 150 V, the current escalated to maximum current, reaching 2.03 µA. At this moment, the Ag particles were almost totally evaporated from the A area of CNF [Fig. 7(f)], however the current suddenly drop to ~300 nA. We believed that the moment before the Ag particles fully evaporated [Fig. 7(f)] there were field electrons emission and thermal electrons emission; two types of electrons emission occurred. The mixture of Ag particles and amorphous carbon induced the joule heat which trigger the thermal emission, thus both electron emission process produced extremely high current at 150 V, 2.03 µA. However, after Ag particles evaporated, the temperature slumped and thermal emission also terminated thus

the emission current flop into 300 nA. Only small portion of amorphous carbon which soluble by the Ag particles transformed into graphitic layers due to the Joule heating which
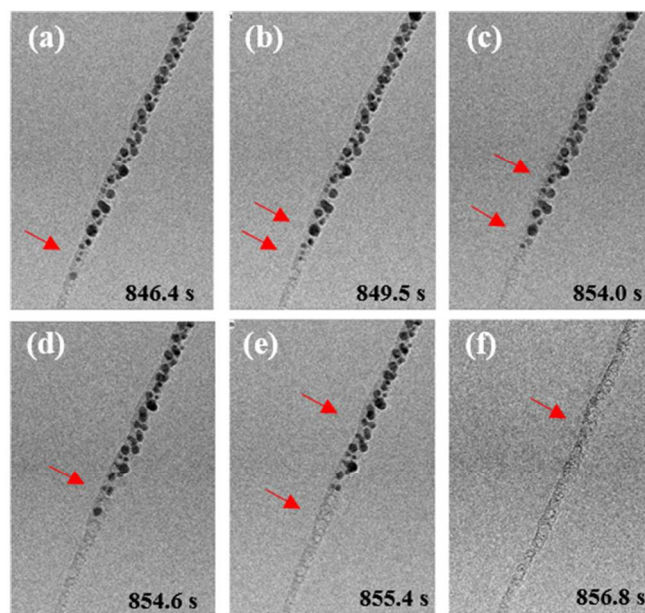
generated during the electron emission process. The melting temperature of carbon nanofiber (~3773 K) is much higher than Ag.[35] Therefore, the structure of the carbon nanofiber were hardly change when it is subjected to a large electric field, while Ag were evaporated due to Joule heating.
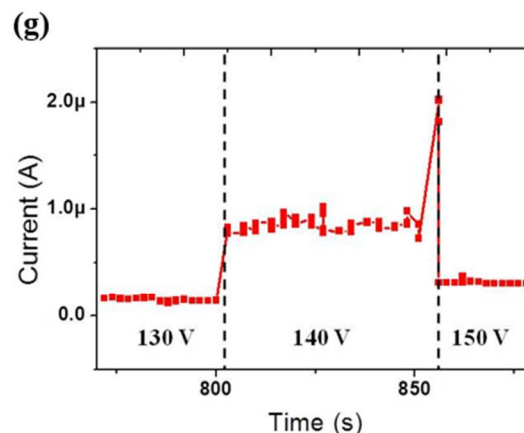

Fig. 7.   (a)-(f) Time-lapsed HRTEM images of Ag-incorporated CNF during field emission process.(g) Current properties of the fiber corresponding to the TEM images.

Conclusions

Transformation of Ag-incorporated CNF structure was observed directly during FE measurement under high current flow between 800 nA to 2.03 µA. The amorphous carbon that surrounding Ag particles were changes to graphene-like structure and the evaporation of Ag particles due to Joule heating effects occurred almost simultaneously, leaving holes

that match the Ag particles size on the fiber part. The Ag particles evaporations leads to the temperature reduction and evacuate the thermal emission thus the emission current sink to ~300 nA. These results also suggest significant information of Ag particles were at poor performance compare to the Ag bulk as catalyst for graphene synthesis.

Acknowledgements

Notes and references

[a] Department of Frontier Materials, Nagoya Institute of Technology, Gokiso-cho, Showa-ku, Nagoya 466-8555, Japan.

Corresponding email: tanemura.masaki@nitech.ac.jp

Tel: +81 52 735 5379, Fax: +81 52 735 5379

[b] Department of Physics, Faculty of Science, Universiti Putra Malaysia, 43400 UPM Serdang, Selangor, Malaysia.

[c] Department of Materials, Faculty of Mechanical Engineering, Universiti Teknologi Malaysia, 81310 Skudai, Johor, Malaysia.

[d] School of Pharmacy, Aichi Gakuin University, Kusumoto-cho, Chikusa-ku, Nagoya 464-8650, Japan.

[e] Department of Chemistry, Faculty of Science and Mathematics, Universiti Pendidikan Sultan Idris, 35900 Tanjong Malim, Perak, Malaysia.

1   K. Geim and K. S. Novoselov, *Nature Mater.*, 2007, **6**, 183.

2   Neto, F. Guinea, N. Peres, K. Novoselov, and A. Geim, *Rev. Mod. Phys.*, 2009, **81**, 109162.

3   Y. Zhang, Y. W. Tan, H. L. Stormer, and P. Kim, *Nature*, 2005, **438**, 201.

4   K. S. Novoselov, A. K. Geim, S. Morozov, D. Jiang, Y. Zhang, S. V. Dubonos, I. V. Grigorieva, and A. A. Firsov, *Science*, 2004, **306**, 666.

5   Lee, X. Wei, J. Kysar, and J. Hone, *Science*, 2008, **321**, 385.

6   M. Liu, X. Yin, E. Ulin-Avila, B. Geng, T. Zentgraf, L. Ju, F. Wang, and X. Zhang, *Nature*, 2011, **474**, 64.

7   K. Kim, J.-Y. Choi, T. Kim, S.-H. Cho, and H.-J. Chung, *Nature*, 2011, **479**, 338.

8   S. Chen, L. Brown, M. Levendorf, W. Cai, S.-Y. Ju, J. Edgeworth, X. Li, C. Magnuson, A. Velamakanni, R. Piner, J. Kang, J. Park, and R. Ruoff, *ACS nano*, 2011, **5**, 1321.

9   L. Gao, J. R. Guest, and N. P. Guisinger, *Nano Lett.*, 2010, **10**, 3512.

10 A. Reina, X. Jia, J. Ho, D. Nezich, H. Son, V. Bulovic, M. S. Dresselhaus, and J. Kong, *Nano Lett.*, 2009, **9**, 130.

11 J. Wintterlin, and M. -L. Bocquet, *Surface Science*, 2009, **603**, 1841.

12 N. Liu, L. Fu, B. Dai, K. Yan, X. Liu, R. Zhao, Y. Zhang, and Z. Liu, *Nano Lett.*, 2011, **11**, 297.

13 X. Li, W. Cai, J. An, S. Kim, J. Nah, D. Yang, R. Piner, A. Velamakanni, I. Jung, E. Tutuc, S. K. Banerjee, L. Colombo, and R. S. Ruoff, *Science*, 2009, **324**, 1312.

14 T. Oznuluer, E. Pince, E. Polat, O. Balci, O. Salihoglu, and C. Kocabas, *Appl. Phys. Lett.*, 2011, **98**, 183101.

15 M. E. Ayhan, G. Kalita, S. Sharma, and M. Tanemura, *Phys. Status Solidi RRL*, 2013, **7(12)**, 1076.

16 D. Takeuchi, Z. P. Wang, K. Yamaguchi, M. Kitazawa, Y. Hayashi, and M. Tanemura, *Journal of Physics: Conference Series*, 2008, **100**, 012029.

17 Z. Wang, M. Z. M. Yusop, T. Hihara, P. Ghosh, A. Hayashi, Y. Hayashi, and M. Tanemura, *Journal of Nanosci. and Nanotech.*, 2011, **11**, 10677.

18 P. Ghosh, M. Z. Yusop, D. Ghosh, A. Hayashi, Y. Hayashi, and M. Tanemura, *Chem. Commun.*, 2011, **47**, 4820.

19 Y. Yaakob, M. Z. Yusop, C. Takahashi, G. Kalita, P. Ghosh, and M. Tanemura, *Jpn. J. Appl. Phys.*, 2013, **52**, 11NL01.

20 M. Z. M. Yusop, Y. Yaakob, G. Kalita, M. Sasase, Y. Hayashi, and M. Tanemura, *ACS Nano*, 2012, **6**, 9567.

21 C. Takahashi, Y. Yaakob, M. Z. M. Yusop, G. Kalita, and M. Tanemura, *Carbon*, 2014, **75**, 277.

22 M. Zamri, P. Ghosh, A. Hayashi, M. Sasase, Y. Hayashi, and M. Tanemura, *J. Vac. Sci. Technol. B*, 2011, **29(4)**, 04E103

23 R. Pasricha, S. Gupta, and A. K. Srivastava, *Small*, 2009, **5**, 2253.

24 M. E. Ayhan, G. Kalita, M. Kondo and M. Tanemura, *RSC Adv.*, 2014, **4**, 26866.

25 C. J. Edgcombe, and U. Valdre, *Journal of Microscopy*, 2001, **203**, 188

26 Z. Xu, X. D. Bai, E. G. Wang, and Z. L. Wang, *Appl. Phys. Lett.*, 2005, **87**, 163106.

27 K. Asaka, M. Karita, and Y. Saito, *Appl. Phys. Lett.*, 2011, **99**, 091907.

28 P. Vincent, S. T. Purcell, C. Journet, and V. T. Binh, *Phys. Rev. B*, 2002, **66**, 075406.

29 J. C. Meyer, A. K. Geim, M. I. Katsnelson, K. S. Novoselov, T. J. Booth, and S. Roth, *Nature Lett.*, 2007, **446**, 05545.

30 H. A. Jones, I. Langmuir, and G. M. J.Mackay, *Phys. Rev.*, 1927, **30**, 201.

31 F. Geiger, C. A. Busse, and R. I. Loehrke, *Int. J. Thermophys.*, 1987, **8**, 425.

32 Q. Jiang, S. Zhang, and M. Zhao, *Mater. Chem. and Phys.*, 2003, **82**, 225.

33 S. Xiao, W. Hu, and J. Yang, *J. Phys. Chem. B*, 2005, **109**, 20339.

34 D. Takagi, Y. Homma, H. Hibino, S. Suzuki, and Y. Kobayashi, *Nano Lett.*, 2006, **6**, 2642.

35 A. G. Whittaker, *Nature*, 1978, **276**, 695

RSC Advances Accepted Manuscript